A Multi-aperture Coaxial Projector Balancing Shadow Suppression and Deblurring

Hiroki Kusuyama, Yuta Kageyama, Daisuke Iwai, and Kosuke Sato

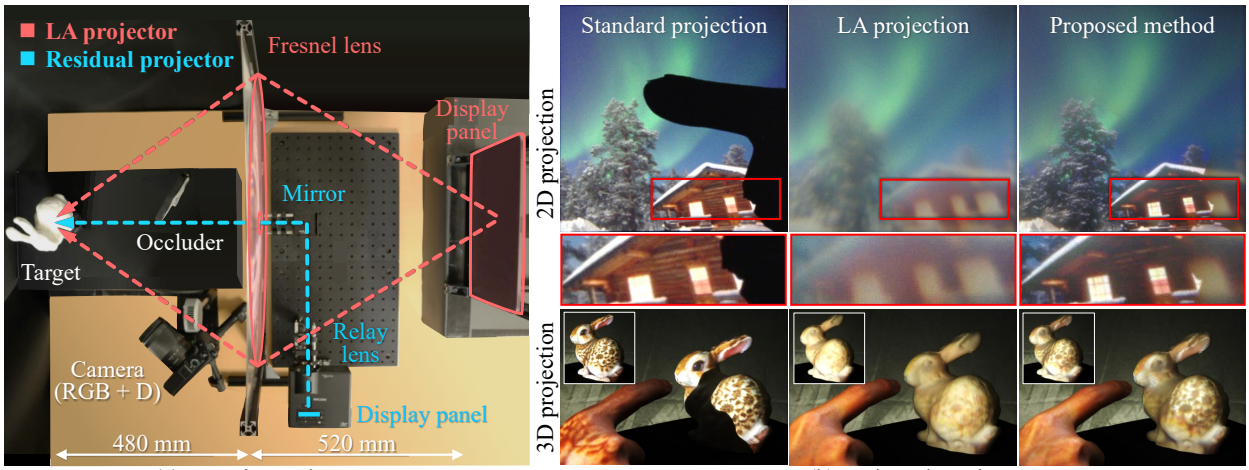

(a) Experimental setup (b) Projected results

Fig. 1: Shadow suppression and deblurring by the multi-aperture coaxial projector: (a) Prototype system consisting of the large-aperture (LA) projector and the residual projector. The LA projector consists of a display panel and an LA Fresnel lens, and the residual projector consists of a display panel, a mirror, and a relay optical system. (b) Projected results in the standard projection, in the LA projection with a conventional deblurring method, and the proposed method. In the standard projection, we cannot see a part of the image due to the cast shadow. In the LA projection, shadows are suppressed; however, the spatial resolution and contrast of the image are significantly low. The proposed system successfully suppresses both the shadow and image quality degradation.

Abstract—This paper proposes a projection system that optically removes the cast shadow in projection mapping. Specifically, we realize the large-aperture (LA) projection using a large-format Fresnel lens to suppress cast shadows by condensing the projection light from a wide viewing angle. However, the resolution and contrast of the projected results are significantly degraded by defocus blur, veiling glare, and stray light caused by the aberration of an LA Fresnel lens. To solve the technical problems, we employ two different approaches: optical and digital image processing methods. First, we introduce a residual projector with a typical aperture lens on the same optical axis as the LA projector, projecting the residual (i.e., high-frequency) components attenuated in the LA projection. These projectors play different roles in shadow suppression and blur compensation, both achieved by projecting simultaneously. Secondly, we optimize the pair of projection images that can balance the shadow suppression and deblurring performance of our projection system. We implemented a proof-of-concept prototype and validated the above-mentioned techniques through projection experiments and a user study.

Index Terms—Human-centered computing—Human computer interaction (HCI)—Interaction devices—Displays and imagers; Computing methodologies—Computer graphics—Graphics systems and interfaces—Mixed / augmented reality

1 Introduction

Projection mapping (PM) realizes spatial augmented reality (AR), seamlessly merging the physical and virtual worlds [6]. It allows for the manipulation of their color and texture by superimposing imagery onto real objects. Unlike video see-through and optical see-through AR, PM enables multiple users to view augmentations on a physical surface without the need to wear or hold any display devices. Users can interact with the projected images once their actions are measured by a PM system. This interactive PM technology finds applications in various fields, such as medicine [42], teleconferencing [18, 46, 48], museum guides [5, 53], makeup [4, 55], object searches [21, 22, 30, 39, 47], product design [8, 37, 40, 59], urban planning [62], and artwork creation [2, 12, 49]. However, in interactive PM, when the users' bodies block the projected light as they approach the target, shadows are cast in the projected results. This problem is a fundamental technical challenge unique to PM. When shadows appear in the projected result, portions of the projected image become invisible, diminishing the user's sense of immersion in the scene [58].

The most common solution for shadow suppression is applying a multi-projection system [20, 23, 24, 29, 41, 43, 57, 60, 61]. Multiple projectors are spatially distributed to project images from a wide range of viewing angles onto the surface of the projection target. When one projector is occluded, a compensating image is generated so that other projectors can cover the area. In most cases, generating compensation images for each projector to achieve geometric and color consistency results in delays in shadow suppression during user interaction. Another approach involves optically suppressing shadows through large-aperture (LA) projection using a large-format optical element. In this optics, light emitted from a display panel is widely spread onto the element,

• *Hiroki Kusuyama, Yuta Kageyama, Daisuke Iwai and Kosuke Sato are with Osaka University. E-mail: see https://www.sens.sys.es.osaka-u.ac.jp.*

Received 14 March 2024; revised 17 June 2024; accepted 1 July 2024.
Date of publication 10 September 2024; date of current version 4 October 2024.
This article has supplementary downloadable material available at https://doi.org/10.1109/TVCG.2024.3456170, provided by the authors.
Digital Object Identifier no. 10.1109/TVCG.2024.3456170

which is then condensed onto the projection surface. As a result, the light is projected from a wide range of incident angles, eliminating the need for computational processing for shadow suppression. In previous work, LA projection has been realized using a micro-mirror array plate (MMAP), a type of retro-transmissive optics [16, 17, 32]. However, their technique requires the preparation of a so-called "proxy object" with a shape that is plane-symmetrical to the projection target, and it needs to be placed plane-symmetrically with the target with respect to the MMAP. Slight changes of the proxy object cause significant degradation of high-frequency components in the projected results. This limitation hinders flexibility in adapting to changes in the target.

In this paper, we propose a novel projection system designed to optically suppress cast shadows while mitigating image quality degradation resulting from changes of the projection target. To achieve this, we employ a large-format lens, specifically a Fresnel lens, offering greater flexibility in accommodating various shapes of the target object without the need for a shape-constrained proxy object, as required in the MMAP approach. This LA projection system suppresses shadows by providing a sufficiently wide aperture visible from any point on the target surface, irrespective of the presence of occluders. On the other hand, the depth-of-field (DOF) of an LA projection system is shallower than that of a projection system with a typical aperture size, leading to defocus blurs in the projected results. Software-based deblurring techniques have addressed this issue [7, 26, 27, 45, 69]. However, they were developed assuming a typical aperture size and there is currently a lack of empirical evidence demonstrating the effectiveness of previous compensation techniques for LA projection systems. Additionally, the Fresnel lens is susceptible to serious aberrations including veiling glare and stray light [14, 33], resulting in a significant reduction in contrast in the projected output.

There are two technical contributions in this paper, addressing the image quality degradation problem in the LA projection system based on a large-format Fresnel lens. As the first contribution, we optically compensate for the degradation by placing another projector with a typical aperture lens so that they share the same optical axis. Specifically, we apply this extra projector for *residual projection*, which overlays the high-frequency components onto the projected result by the LA projector. This projection setup achieves both shadow suppression and mitigation of image quality degradation in non-shadow areas. However, both performances cannot be simultaneously maximized. In other words, increasing the projected image quality by assigning a higher weight to the residual projection results in a deterioration of shadow suppression performance, and vice versa. Therefore, as the second contribution, we present an optimization framework that balances the trade-off demands in generating projection images for both LA projection and residual projection. Similar to previous techniques, we model a projected result as the convolution of an original image and a spatially varying point spread function (PSF). However, in contrast to prior methods, we utilize a mixture of Student's t-distribution to represent the PSF for the LA projection. The t-distribution, characterized by heavier tails, more accurately captures the PSF of a projection system using a Fresnel lens, which is susceptible to veiling glare and stray light, than the typical Gaussian distribution. Our optimization framework simultaneously optimizes images for both LA projection and residual projection by minimizing the error between the target appearance and the projected result estimated by the convolution. Additionally, it offers users the flexibility to adjust the balance between improving image quality and enhancing shadow suppression performances.

This paper provides a detailed explanation of the mathematical model and computational algorithm employed in the proposed method. Subsequently, experimental results from a prototype system are presented, demonstrating the validity of our PSF model in approximating the optical characteristics of the proposed projection system. The results also illustrate the effectiveness of the proposed technique in achieving a balance between shadow suppression performance and image quality enhancement. Furthermore, a user study validates the efficacy of the proposed method in a practical usage scenario.

Our primary contributions are that we:

- develop a novel projection system that optically suppresses cast shadows and mitigates the image quality degradation in non-shadow areas,
- model the degradation in the projection with an LA Fresnel lens more accurately than previous methods,
- design an optimization framework for generating the pair of projection images that balances the shadow suppression and deblurring,
- demonstrate the validity of our PSF model and our generation method for projection images through projection experiments,
- validate the efficacy of the proposed method in a practical usage scenario through a user study.

2 Related Work

2.1 Shadow suppression in PM

PM systems are susceptible to occluders blocking the projection light. Theoretically, when the apparent size of the projector's aperture seen from the projection surface exceeds the size of the occluder, shadows will be suppressed. Advancements in shadow suppression in PM have been achieved by adopting synthetic-aperture projection techniques that distribute multiple projectors over a projection target to ensure that users cannot occlude the projected content from any angle. Whenever a camera detects an occluder [1, 20, 29, 43] or its shadow [23, 24, 56, 57, 60, 61], the system covers the occluded area by illuminating it from unoccluded projectors. Multi-projection systems have also been developed using mirror arrays, with each mirror functioning as a distributed projector, efficiently reflecting the image from a single projector onto the target [34, 41]. However, the synthetic aperture methods are susceptible to computational delays and cannot completely eliminate shadows when occluders are in motion.

On the other hand, shadows can be eliminated without delay in an LA projection system using a large-format optical element. In previous research, retro-transmissive optics known as an MMAP were employed to achieve shadowless projection. Because the MMAP is a reflection-based optical element, it theoretically avoids aberrations even in a large format. Previous work applied an MMAP over a 450 mm square [16, 17, 32]. However, as discussed in section 1, the MMAP-based system requires a proxy object that needs to be perfectly plane-symmetric to each projection target. This inflexibility heavily constrains the shape and the six degrees of freedom pose of the target object to those of the proxy object. Additionally, the MMAP is not a dioptric lens, and thus, we cannot implement functions typical of optical lens-based projection systems, such as zooming.

2.2 Fresnel lens in AR/VR displays

A Fresnel lens is composed of a series of concentric annular sections, replicating the optical characteristics of a conventional lens. A spherical Fresnel lens is functionally similar to a basic spherical lens, utilizing ring-shaped segments, each representing a portion of a sphere, to converge light onto a single point. This design allows for a significant reduction in thickness, even for a large aperture and short focal length lens. Due to this advantage, Fresnel lenses are commonly used as eyepieces in AR and virtual reality (VR) headsets [3, 25]. However, the thin form factor comes at the cost of a potential reduction in image quality. While a Fresnel lens can form an image, the resulting image may not be as clear as that formed by an equivalent simple spherical lens due to diffraction at the edges of the ridges [14, 33]. The resulting veiling glare and stray light cause a significant deterioration in the contrast and sharpness of the displayed image in the headsets. While there are optical solutions to mitigate undesirable diffraction, they require tailored fabrication of light-shielding films, which are not usually available in consumer-level AR/VR systems [15, 51].

Considering the thin form factor, we believe that a large-format Fresnel lens is a promising replacement for the MMAP in an LA projection system to achieve a similarly high shadow suppression performance. However, we need to solve the inherent problem of the Fresnel lens

to realize a PM system that can form a sharp and clear image in projected results without suffering from the above-mentioned image quality degradation.

2.3 Projector deblurring

Projector deblurring techniques potentially alleviate the significant degradation in the contrast and sharpness of projected results in a Fresnel lens-based LA projection system. They address defocus blur in a typical PM system by generating compensation images through modeling the image quality degradation process and solving its inverse problem. Previous studies applied the convolution of the original image and a spatially-varying PSF to the image quality degradation model. The simplest solution for its inverse is applying the Wiener filter that amplifies the high-frequency components of the original image, which compensates for the blur in the projected result [7,45]. However, this technique suffers from the presence of values near zero in the high-frequency components of the PSF and the limited dynamic range of the projector, resulting in the occurrence of ringing artifacts in the projected result. The artifacts can be alleviated by employing a constrained optimization method as a replacement for the Wiener filter [69]. Recent studies achieved real-time optimization computation by applying deep neural networks [26,27].

The primary limitation of these previous techniques is that they assumed a Gaussian distribution as the PSF. This assumption is valid as long as we address defocus blur problems for projectors with typical spherical lenses. However, the blur-like image quality degradation in a Fresnel lens-based LA projection system does not solely suffer from defocus as discussed in subsection 2.2, and thus, the Gaussian distribution does not accurately represent its PSF. Although there is a technique that does not assume any distribution model for the PSF [66], it requires a long measurement time (e.g., two hours [54]) for the light transport matrix. More critically, even if we can use an accurate PSF in the compensation computation, it is physically impossible for these solely software-based techniques to recover high-frequency components that are missing through the projection process, due to the limited dynamic range of the projector.

2.4 Our contributions over prior studies

In this paper, we propose an LA projection system that optically suppresses shadows in PM without delays by employing a large-format acrylic Fresnel lens, which is flexible for changes in the shape and pose of a projection target. Considering the technical limitations of software-based projector deblurring techniques, we employ a hardware-based solution to address the image quality degradation issue in our PM system. Specifically, we employ another projector with a typical aperture lens coaxially with the LA projector and compensate for the missing high-frequency components in projected results. Furthermore, we propose an optimization framework that computes projection images for both projectors while balancing the shadow suppression and image quality enhancement performances. We apply a more accurate PSF model in the optimization framework than the previous techniques.

3 A Multi-aperture Coaxial Projector

Our proposed PM system achieves both shadow suppression and the mitigation of image quality degradation. The system consists of two different types of projectors: the *LA projector* and the *residual projector* (Figure 2). The LA projector consists of an LA Fresnel lens and a display panel, and is primarily responsible for shadow suppression. Light rays emitted from each pixel of the display panel are concentrated on a projection target by refraction of the LA Fresnel lens. By employing a lens that is sufficiently wider than the occluder, the projector effectively suppresses cast shadows. However, the high-frequency components in the projected results are attenuated due to defocus blur, veiling glare and stray light occurring in the LA Fresnel lens.

In contrast, the residual projector consists of lenses with a typical aperture and a display panel, and compensates for high-frequency components that are attenuated in the LA projection. Residual projection is advantageous for projecting high-frequency components due to the relatively small lens aperture, producing a clear image. Additionally, the small numerical aperture results in a wide DOF. Projection with these two projectors achieves both shadow suppression and deblurring. In areas where the residual projection is occluded, the projected result appears blurred; however, the color and texture roughly remain. We believe this is more preferable than causing umbras in terms of user experience.

These two projectors need to be aligned along the same optical axis to release the bothersome and error-prone geometric registration. In conventional projector-camera systems, coaxial systems have been implemented by using a half mirror or a beam-splitter [13,67]. However, directly adopting this method would require a half mirror as large as the LA Fresnel lens. A naïve alternative is to place the residual projector in front of or behind the Fresnel lens, while aligning its optical axis with that of the LA projector (Figure 2 (b)). However, the projected result becomes dark due to the occlusion of the LA projection by the housing of the residual projector.

Therefore, we minimize this occlusion by positioning the display panel and housing of the residual projector outside the Fresnel lens and relaying the display panel using a narrow optical system (Figure 2 (c)). The optical axes and optical centers of the two projectors are aligned by reflecting the projection light from the residual projector with a mirror placed at the center of the Fresnel lens.

4 Software-based Deblurring

In our projection system, the LA projector suppresses shadows and the residual projector mitigates the image quality degradation, but these performances cannot be maximized simultaneously. In the residual projection, the occluder casts an umbra as in a typical projection. Therefore, a better shadow suppression performance is achieved by decreasing the contribution of the residual projection. However, this leads to an image quality degradation. To alleviate it, we maximize the image quality of the LA projection results to achieve the upper limit of the displayable image quality. Specifically, the high spatial frequency components of the projected result are significantly attenuated in the LA projection, and thus, the projection image for the LA projector should be sharpened. Furthermore, it is preferable for the shadow suppression and deblurring performance of the projection system to be adjustable according to applications. We formulate an optimization problem based on these requirements and solve it to generate projection images for the two projectors.

4.1 PSF model of LA projection

The defocus blur in PM can be modeled as the convolution of PSF h as follows:

$$I_B = h \otimes I_P, \tag{1}$$

where I_P and I_B represent the projection image and the resultant blurred image respectively, and $\otimes$ is the convolution operator. Suppose the target image in the projected scene is T. Solving the inverse problem of Equation 1 so that the projected result I_B approaches T yields the *compensation image* I_P^*.

$$I_P^* = h^{-1} \otimes T. \tag{2}$$

To generate projection images for deblurring, it is imperative to precisely model the PSF of the projection system. The PSF is measured as the spatial luminance distribution of a projected dot pattern and is typically modeled using a Gaussian distribution h_g as:

$$h_g(\mathbf{x} \mid \boldsymbol{\mu}, \boldsymbol{\Sigma}) = \frac{1}{2\pi\sqrt{|\boldsymbol{\Sigma}|}} \exp\left\{ -\frac{1}{2}(\mathbf{x}-\boldsymbol{\mu})^\top \boldsymbol{\Sigma}^{-1}(\mathbf{x}-\boldsymbol{\mu}) \right\}, \tag{3}$$

where $\mathbf{x}$, $\boldsymbol{\mu}$, and $\boldsymbol{\Sigma}$ represent the pixel coordinate, the mean position of the distribution, and the variance-covariance matrix of the distribution, respectively. Although this model has been commonly used in previous research, it accounts only for degradation in a projector with a typical spherical lens, such as defocus blur [7,11].

In the LA lens, its shallow DOF greatly increases the defocus blur. Additionally, not only defocus blur, but also undesirable veiling glare

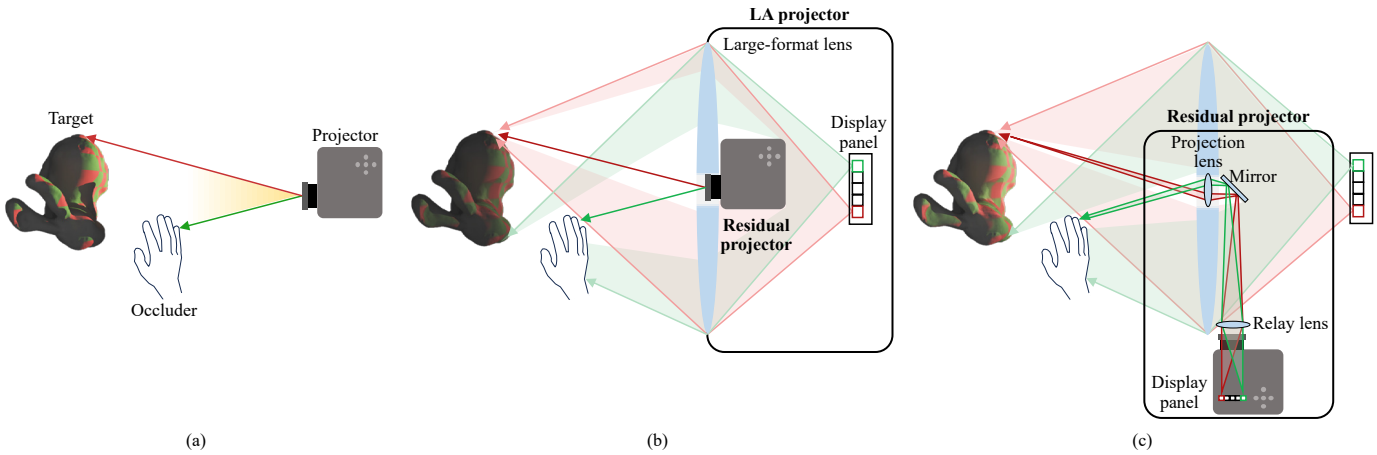

Fig. 2: The principle of shadow suppression and mitigation of image quality degradation by the multi-aperture coaxial projector. (a) When using the typical projector, the occluder casts shadows on the projection target. (b) In coaxial projection, the LA projector suppresses shadows and the residual projector compensates for high-frequency components attenuated in the LA projection. However, much of the projection light from the LA projector is occluded by the housing of the residual projector. (c) Proposed projection system. The display panel of the residual projector and its housing are positioned outside the Fresnel lens. The display panel is relayed by a small optical element to minimize the occlusion of the LA projection.

and stray light occurring in the LA Fresnel lens cause blur. This blur has an impact on an extremely wide spatial area and it attenuates the high-frequency components in the projected result. To deal with these extensive blur, we apply a heavy-tailed distribution compared to the Gaussian distribution. Therefore, we use a t-distribution h_t in the PSF model of the LA projector.

$$h_t(\mathbf{x} \mid \boldsymbol{\mu}, \boldsymbol{\Sigma}, \nu) = \frac{1}{\nu\pi\sqrt{|\boldsymbol{\Sigma}|}} \frac{\Gamma(\frac{\nu+2}{2})}{\Gamma(\frac{\nu}{2})} \left\{ 1 + \frac{(\mathbf{x}-\boldsymbol{\mu})^\top \boldsymbol{\Sigma}^{-1} (\mathbf{x}-\boldsymbol{\mu})}{\nu} \right\}^{-\frac{\nu+2}{2}}, \tag{4}$$

where ν represents the degrees of freedom for the t-distribution and $\Gamma(\cdot)$ represents the gamma function.

To model the PSF accurately, we decompose the blur produced by the LA projector into defocus blur and diffraction in the Fresnel lens. We map a t-distribution with a different variance-covariance matrix to each type of blur, and use a mixture of these distributions to represent the PSF.

$$\begin{aligned} h(\mathbf{x} \mid \boldsymbol{\mu}, \boldsymbol{\Sigma}, \sigma, \alpha) \\ = \alpha h_t^1(\mathbf{x} \mid \boldsymbol{\mu}, \boldsymbol{\Sigma}, 1.5) + (1-\alpha) h_t^2(\mathbf{x} \mid \boldsymbol{\mu}, \sigma \boldsymbol{E}, 1.5), \end{aligned} \tag{5}$$

where h_t^1 and h_t^2 represent the t-distribution for defocus blur and diffraction in the Fresnel lens respectively, and h is the PSF of the LA projector. σ represents the variance and $\boldsymbol{E}$ represents the identity matrix, and we assume isotropy in h_t^2. Since veiling glare and stray light generally affect a wider area than defocus blur, the variance of h_t^2 is larger than that of h_t^1. In this paper, we experimentally set the degrees of freedom of the t-distribution to 1.5. By using the parameter α $(0 \leq \alpha \leq 1)$, two t-distributions are blended in the ratio $\alpha : 1-\alpha$.

4.2 Projection image generation

We generate the compensation images by solving the inverse problem described in Equation 2 with the proposed PSF model. Convolution in the spatial domain can be reformulated as a multiplication in the frequency domain. Therefore, this inverse problem can be solved as a division in the frequency domain.

$$\mathscr{F}(I_P^*) = \frac{\mathscr{F}(T)}{\mathscr{F}(h)}, \tag{6}$$

where $\mathscr{F}(\cdot)$ is the Fourier transform. The compensation image can be obtained by applying the inverse Fourier transform to $\mathscr{F}(I_P^*)$. However, h is substantively a low-pass filter and its Fourier representation $\mathscr{F}(h)$ contains many near zeros in the high-frequency components, which results in the strong ringing artifacts.

In previous research [69], the ringing problem has been addressed by iteratively solving a constrained optimization problem as follows:

$$I_P^* = \arg\min_{I_P} \quad ||T - f(I_P)||^2, \tag{7a}$$

$$\text{subject to} \quad \forall \mathbf{x},\ 0 \leq I_P(\mathbf{x}) \leq 255, \tag{7b}$$

where $\mathbf{x}$ represents the pixel coordinates of the projector and $f(\cdot)$ represents the degradation function based on the PSF. Equation 7b imposes a constraint on the dynamic range of the projector (i.e., 8 bits). We extend this optimization method to generate two projection images for the LA projector and the residual projector.

An overview of the projection image generation flow is shown in Figure 3. The proposed generation method consists of three main steps: PSF estimation, optimization calculations and addressing spatial-varying PSFs.

4.2.1 PSF estimation

In the 3D PM, the PSF varies spatially due to different depth values at each point on the 3D target surface. In the LA projection, this becomes more significant due to shallow DOF. Additionally in the Fresnel lens, acquired PSFs vary even at the same depth due to the effects of veiling glare and stray light [14].

Therefore, as the first step of our generation method, we acquire distinct PSFs by projecting a dot pattern onto a white planar screen placed at n different depths $z_1, \cdots, z_n$. Suppose the number of dots in a dot pattern is m, we acquire m distinct PSFs at each depth. Next, the PSF model shown in Equation 5 is fitted to each of the acquired PSFs. These $n \times m$ estimated PSFs are input to the optimization solver one by one with the target image.

4.2.2 Optimization of projection images

In our proposed projection system, the contribution of residual projection should be minimized, as its light is entirely blocked by an occluder. Therefore, we optimize the projection image for the LA projector through deblurring to reproduce a target image as closely as possible using only the LA projection. Based on Equation 7, we formulate the optimization problem as follows:

$$I_{LA}^*, I_R^* = \arg\min_{I_{LA}, I_R} \begin{cases} ||T_{LA} - f(I_{LA})||^2, & \text{(8a)} \\ ||T - f(I_{LA}) - I_R||^2 + \lambda ||I_R||^2, & \text{(8b)} \end{cases}$$

$$\text{subject to} \quad \forall \mathbf{x},\ 0 \leq I_{LA}(\mathbf{x}), I_R(\mathbf{x}) \leq 255, \tag{8c}$$

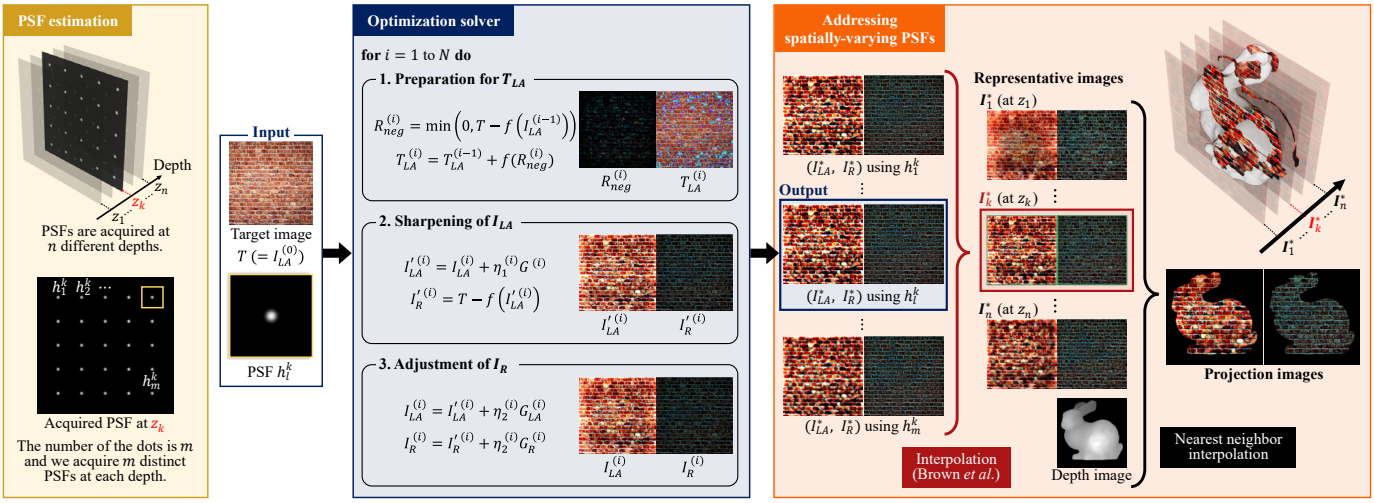

Fig. 3: Generation flow of the projection images addressing the spatially-varying PSFs.

$$T - f(I_{LA}) \geq 0, \tag{8d}$$

where I_{LA} and I_R represent the projection images for the LA projector and the residual projector, respectively, and I_{LA}^* and I_R^* represent their optimized results.

Equation 8d ensures that residuals between the target image and the projected result of the LA projector remain non-negative. Basically, the residual projector is responsible for projecting these residuals. However, since projectors cannot produce negative luminance, it is crucial to avoid negative residuals during the subtraction process. Negative residuals are caused by luminance flowing into a pixel from its surrounding pixels due to blur. Therefore, we reduce the luminance of the target image for the LA projector in the pixels where negative residuals occur and its surroundings. To achieve this, we introduce a separate target image T_{LA} for the LA projection, a darker version of the original target image T. The initial value of T_{LA} is set to T. We compute R_{neg}, which is an image consisting only of negative residuals (Equation 9a). To reduce luminance in the surrounding pixels as well, the degradation function $f(\cdot)$ is applied to R_{neg}, and this is used to reduce the luminance of T_{LA} (Equation 9b).

$$R_{neg} = \min(0, T - f(I_{LA})), \tag{9a}$$

$$T_{LA} = T + f(R_{neg}). \tag{9b}$$

Equation 8a enhances the spatial frequency components of the LA projector to compensate for the blur, and Equation 8b brings the projected result closer to the target image in projection using the two projectors. The constant $\lambda (\geq 0)$ adjusts the contribution of the residual projector, balancing between shadow suppression and deblurring performance. The larger the value of λ, the better the shadow suppression performance. Conversely, the smaller the value, the better the image quality.

To solve this optimization problem, we use an iterative constrained steepest descent algorithm. In the previous research, the degradation function $f(I_P)$ is represented as $\mathbf{HI_P}$, a matrix multiplication in the spatial domain [69]. $\mathbf{H}$ is the light transport matrix and $\mathbf{I_P}$ is the projection image in column vector form. Each row of $\mathbf{H}$ represents the PSF of the corresponding pixel. However, the calculation for the light transport matrix $\mathbf{H}$ is computationally costly. Therefore, in our implementation, we represent the convolution of the PSF h as the multiplication in the frequency domain, and $f(I_{LA}) = \mathscr{F}^{-1}(\mathscr{F}(h)\mathscr{F}(I_{LA}))$.

The specific process flow is outlined in Algorithm 1 where G is the gradient term, η is the learning rate, and clamp$(\cdot)$ represents a pixel-wise clamp operation that projects values below 0 to 0 and values above 255 to 255 in 8-bit representation. The number of iterations N is set to 10. Lines 2 to 7 of the algorithm aim at minimizing the objective function stated in Equation 8a. Line 3 updates the target image for the LA projector T_{LA} using R_{neg}. Line 6 updates the projection image for the LA projector within the dynamic range using the obtained T_{LA}. Line 7 generates the projection image for the residual projector by computing residuals between the target image and the projected result of the LA projector. Lines 8 to 12 focus on minimizing the objective function presented in Equation 8b.

Algorithm 1 Generation algorithm for projection images

Input: $I_{LA}^{(0)} = T_{LA}^{(0)} = T$
Output: I_{LA}^*, I_R^*

1: **for** $i = 1$ to N **do**
2: $R_{neg}^{(i)} \leftarrow \min(0, T - f(I_{LA}^{(i-1)}))$
3: $T_{LA}^{(i)} \leftarrow T_{LA}^{(i-1)} + f(R_{neg}^{(i)})$
4: $G^{(i)} \leftarrow f((T_{LA}^{(i)} - f(I_{LA}^{(i-1)})))$
5: $\eta_1^{(i)} \leftarrow ||G^{(i)}||^2 \,/\, ||f(G^{(i)})||^2$
6: $I_{LA}^{\prime(i)} \leftarrow \text{clamp}(I_{LA}^{(i)} + \eta_1^{(i)} G^{(i)})$
7: $I_R^{\prime(i)} \leftarrow \text{clamp}(T - f(I_{LA}^{\prime(i)}))$
8: $G_{LA}^{(i)} \leftarrow f((T - f(I_{LA}^{\prime(i)}) - I_R^{\prime(i)}))$
9: $G_R^{(i)} \leftarrow T - f(I_{LA}^{\prime(i)}) - (1+\lambda) I_R^{\prime(i)}$
10: $\eta_2^{(i)} \leftarrow ||G_{LA}^{(i)}||^2 \,/\, 2||f(G_{LA}^{(i)})||^2$
11: $I_{LA}^{(i)} \leftarrow \text{clamp}(I_{LA}^{\prime(i)} + \eta_2^{(i)} G_{LA}^{(i)})$
12: $I_R^{(i)} \leftarrow \text{clamp}(I_R^{\prime(i)} + \eta_2^{(i)} G_R^{(i)})$
13: **end for**
14: **return** $I_{LA}^* = I_{LA}^{(N)}$, $I_R^* = I_R^{(N)}$

4.2.3 Addressing spatially-varying PSFs

The above-mentioned optimization solver outputs the pair of compensation images (i.e., I_{LA}^*,I_R^*) from one PSF; however, it only works with a spatially-uniform PSF. As described in subsubsection 4.2.1, the PSFs of our projection system have the spatially-varying characteristics. Therefore, we interpolate the optimized images within and between depths, respectively.

First, we interpolate the optimized images within the same depth. As the output of the solver, we obtain m pairs of compensation images at a given depth z_k $(1 \leq k \leq n)$. Using these images, we generate the *representative image*, which is the compensation image corresponding to each depth while addressing the spatially-varying PSFs in the method of Brown et al [7]. In this method, the pixel values in the representative

image are determined by bilinear interpolation of the output images of the solver using the four closest neighbor PSFs. This process is performed at each depth to generate n representative images.

Next, we perform interpolation in the depth direction to generate the final projection images. In this paper, five depth planes were placed at intervals of 20 mm so that there is a significant difference in the variance of the PSF between two adjacent planes. We obtain the depth of the projection target using a depth camera and generate the corresponding projection image. We determine each pixel in the projection image by nearest neighbor interpolation with respect to the depth direction. Specifically, each pixel value in the projection image is the value of the corresponding pixel in the representative image at the nearest depth. Note that if the representative images are computed in advance, our method is computationally low-cost because all that needs to be done during projection is the acquisition of the depth values and nearest neighbor interpolation.

5 Projection Experiment

5.1 Experimental setup

We built a prototype to validate the principles of shadow suppression and blur compensation (Figure 1). We achieved coaxial projection by determining the focal length and rough position of the lenses using the lens formula, followed by making fine adjustments manually. This ensures that the optical centers and the projected image sizes correspond between the LA projector and the residual projector.

We implemented the LA projector using an LA Fresnel lens (SIGMA-KOKI, FRLN-500S-250P, diameter: 500 mm) and a flat panel display (Apple, iPad Pro 12.9 inch 5th generation, 2732×2048 pixels). In the center of the Fresnel lens, we drilled a hole with a diameter of 30 mm to prevent the projection light from the residual projector from entering the Fresnel lens. The display panel of the residual projector was transferred using a relay optical system consisting of several lenses, a mirror (Thorlabs, CCM1-PBS251/M), and a projector (RICOH, PJ WXC1110, resolution: 1280×800 pixels, panel size: 0.45 inch). The projector was disassembled, and the built-in objective lens was removed. The relay optical system consists of lenses with focal lengths of 40 mm (Thorlabs, AC254-040-A), 50 mm (Thorlabs, AC254-050-A), and 100 mm (Thorlabs, AC254-100-A). We used an RGB camera (Canon, EOS M6 Mark Ⅱ, 6960×4640 pixels) to capture the projected images, and an RGBD camera (Intel, Real Sense L515, Depth: 1280×720 pixels) to acquire depth values of the projection surface.

5.2 PM onto 3D objects

We implemented a 3D PM using the proposed system. We prepared a 3D-printed Stanford bunny (height: 110 mm) as the projection target. We considered three different projection conditions: standard projection, LA projection, and our proposed method. In the standard projection, the residual projector projected the target image, while the LA projector was turned off. In the LA projection, the LA projector projected the image computed by the standard deblurring method of Zhang and Nayer [69] with our PSF model (Equation 5), while the residual projector was turned off. In our proposed method, we computed projection images using our optimization method with λ of 0.

We examined the projected results in terms of the presence of shadows and image quality in a situation where a human hand approached the target object. The projected results are shown in Figure 1. Our proposed method successfully suppressed shadows caused by occlusion and produced clearer images compared to the LA projection.

5.3 Validation of PSF model

To validate the PSF model described in subsection 4.1, we measured the PSF of the LA projector. We projected a 5×5 dot pattern onto a white planar screen located 480 mm away from the Fresnel lens. The dots were spaced 100 pixels apart horizontally and vertically, resulting in a dot pattern image size of 500×500 pixels. The image captured by the camera is shown in Figure 4(a). We fitted the obtained PSFs with both the conventional model (Equation 3) and our model (Equation 5) using the Levenberg-Marquardt algorithm [38]. Figure 4(b) shows the intensity distribution along the x-axis in the highlighted block from Figure 4(a). Unlike the conventional model, our model represents a distribution that closely matches the actual PSF. The distribution of our model is closer in terms of the heavy-tailed characteristics of actual PSFs, which validates its accuracy.

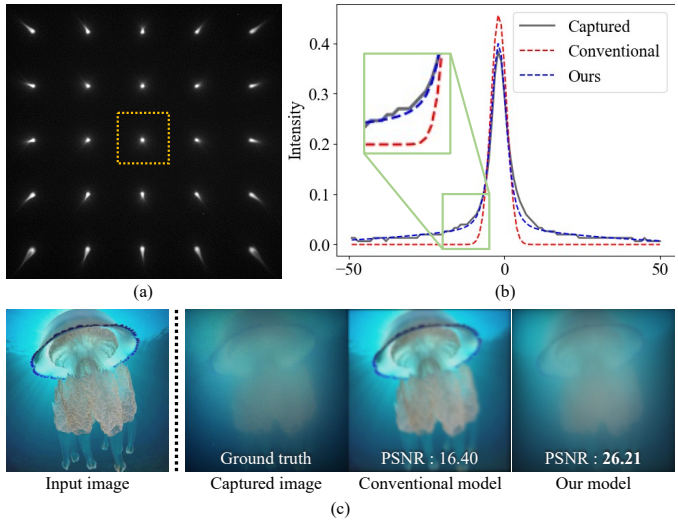

Fig. 4: Results of the PSF estimation. (a) Projected dot pattern by LA projector. (b) Intensity distribution along the x-axis for the block shown in yellow in (a). (c) Comparison of the projected result on the simulation between the conventional model and our model. From left to right: image input to the projector, projected results of the actual LA projector, simulated results using the conventional model, and simulated results using our model.

Using a natural image, we confirmed that our model accurately models the blur in the LA projection compared to the conventional model. Figure 4(c) illustrates the projected results of a natural image using the actual LA projector and the simulated results using both the conventional and our models. Our model provides images that exhibit closer contrast and sharpness to the actual captured images. The similarity between the actual projected results and the simulated results of the two models was evaluated using the Peak Signal to Noise Ratio (PSNR). The result demonstrates that our model consistently produces the image closer to the actual captured image, and provides quantitative evidence of the effectiveness of our model.

5.4 Evaluation of projected image quality and shadow suppression performance

We validated the shadow suppression and deblurring performance of our proposed projection system. We prepared 20 target images of 400×400 pixels by selecting images of plants, animals, and landscapes from the ImageNet dataset [9]. Using the estimated PSF from subsection 5.3, we generated projection images for both LA projection and residual projection. Note that the luminance of the input image for the LA projector T_{LA} compared to the original target image T was 74 percent ($\lambda = 0$) and 77 percent ($\lambda = 0.5$) on average of 20 images. To compare projected results under different experimental conditions, we prepared two conditional factors: the projection and the occluder factors. There were eight conditions in the projection factor and two conditions in the occluder factor, making a total of 16 (= 8×2) conditions.

Projection factor: The first condition is denoted as *Standard*, where the residual projector with a typical aperture lens projected the target image, while the LA projector was turned off. The second condition is denoted as *Synthetic*, where the residual projector and another standard projector (Optoma, ML1050ST+S1J, resolution: 1280 × 800 pixels, panel size: 0.45 inch) projected the image with half the luminance of the target image, while the LA projector was turned off. The third condition is denoted as *LAonlyUncompen*, where the LA projector projected the target image without any compensation, while the residual projector was turned off. The fourth and fifth conditions

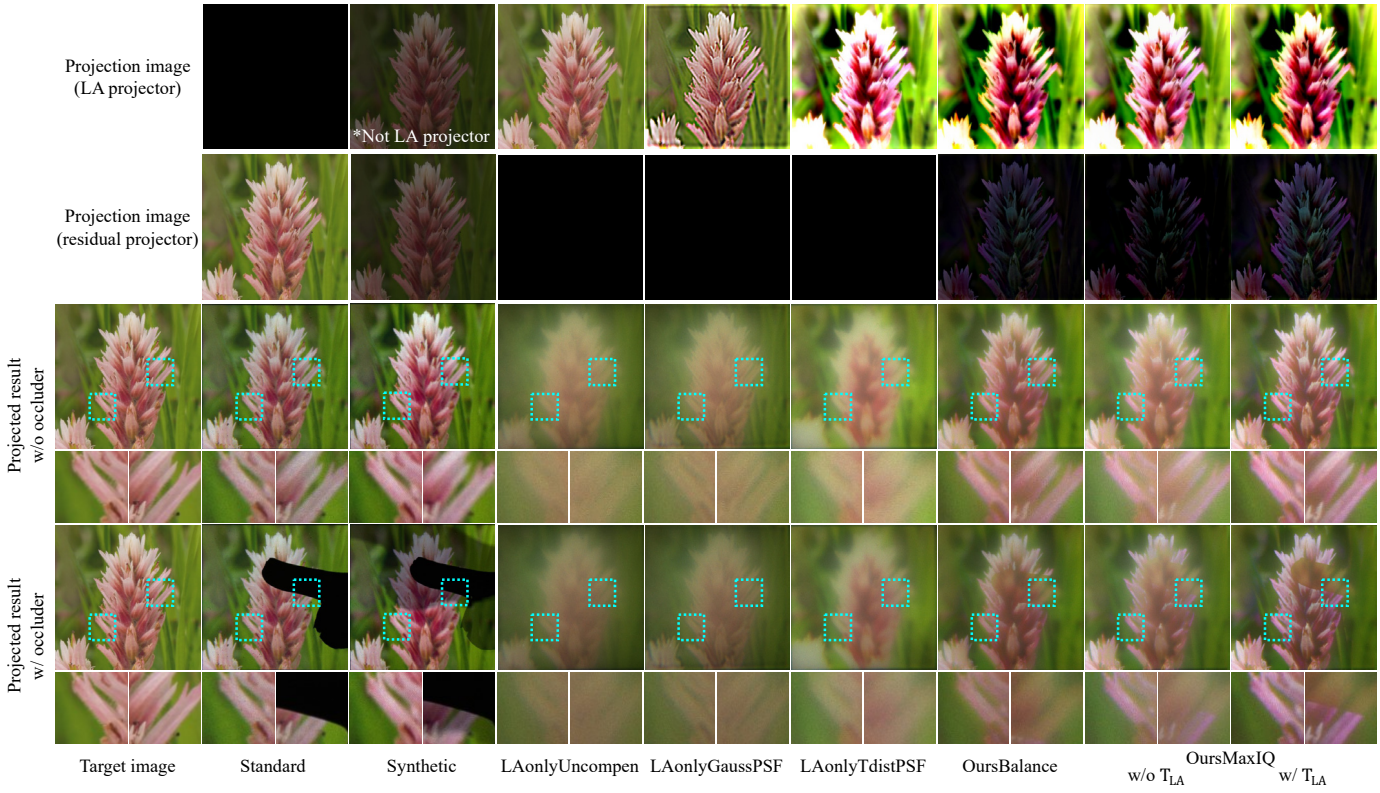

Fig. 5: Comparison of projected results under different projection and occluder conditions. The projection images for the LA and residual projectors are shown in the first and second lines from the top, respectively. The third and fourth lines are the projected results onto a white planar surface without and with an occluder.

Table 1: Average of the image quality evaluation values of the projected results for 20 images under different projection and occluder conditions.

Metrics	Occluder factor	Projection factor: Standard	Synthetic	LAonly Uncompen	LAonly GaussPSF	LAonly TdistPSF	Ours Balance	OursMaxIQ w/o T_{LA}	OursMaxIQ w/ T_{LA}
PSNR (↑)	w/o	20.95	20.74	16.84	17.24	17.83	21.40	19.80	**22.31**
	w/	13.57	12.78	14.29	14.87	17.65	16.87	**19.37**	18.31
SSIM (↑)	w/o	0.600	**0.634**	0.419	0.435	0.415	0.582	0.510	0.632
	w/	0.521	0.465	0.410	0.429	0.427	0.542	0.502	**0.584**
DISTS (↓)	w/o	**0.143**	0.159	0.441	0.382	0.385	0.230	0.283	0.183
	w/	0.245	0.258	0.477	0.416	0.409	0.259	0.302	**0.217**

are denoted as *LAonlyGaussPSF* and *LAonlyTdistPSF*, respectively. In both conditions, the projection image is computed by using the standard deblurring method of Zhang and Nayer [69]. The conventional Gaussian distribution was used in the LAonlyGaussPSF condition, and our PSF model using t-distribution was applied in the LAonlyTdistPSF condition. The remaining conditions are denoted as *OursBalance* and *OursMaxIQ*. We computed projection images with λ of 0.5 in the OursBalance condition, and with λ of 0 in the OursMaxIQ condition, which maximizes the image quality. To demonstrate the effect of introducing T_{LA}, the OursMaxIQ condition was divided into two: without and with T_{LA}.

To ensure color consistency between the target appearance and captured images, we applied color correction [68]. We estimated an unknown 3×4 matrix for applying the color correction by capturing the projected uniform color patterns of 27 different colors. This matrix was computed for each of the LA and residual projectors and applied to computing each projection image.

Occluder factor: The first condition is *without* occluder, and the second condition is *with* occluder. In the condition with occluder, we placed a human-hand-like occluder with a finger width of approximately 8 mm at a distance of 250 mm from the target object.

The projection images and projected results for each condition are shown in Figure 5. The image quality of the projected results was evaluated using the PSNR, Structural SIMilarity (SSIM) [65] and Deep Image Structure and Texture Similarity (DISTS) [10] metrics. We calculated the average quality evaluation scores for the 20 images in all conditions, and the results are shown in Table 1.

In the Standard condition, we obtained a clear image, but the occluder caused some parts of the projected image to be completely invisible due to an umbra. In the synthetic condition, the synthetic aperture reduced the size of the umbra area, but caused areas of lower luminance compared to the surroundings (penumbra). In the LAonlyUncompen condition, the shadows caused by the occluder were no longer visible, but there was a significant decrease in resolution and contrast. In the LAonlyGaussPSF condition, there was a slight improvement in resolution, but the contrast remained low. In the LAonlyTdistPSF condition, there was a slight improvement in contrast, but the resolution was lower than the LAonlyGaussPSF condition. In the OursBalance

and OursMaxIQ conditions, which utilized the residual projector, we successfully improved the sharpness of the images while preserving the shadow suppression performance. It is worth mentioning that OursMaxIQ produced high-quality images in non-shadowed areas, while OursBalance exhibited the characteristic of less perceptible shadows. Additionally, in the condition with T_{LA}, the SSIM and DISTS values, which represent human perception better than PSNR, were higher than in the condition without T_{LA}. This result provides validity for the introduction of T_{LA}.

In all metrics, our proposed methods improved image quality compared to all LAonly conditions. These results provide significant quantitative evidence that adding a residual projector greatly enhances the image quality of the projected results. It is worth noting that partial image loss caused by shadows affected image quality in all metrics. Nevertheless, our proposed methods successfully reduced the luminance reduction in shadow areas, resulting in less image quality degradation compared to standard projection.

6 User Study

We conducted a user study on hand interactive PM to investigate how the proposed method affects task performance. In interactive PM in the industrial and medical fields, multiple users attempt to touch the projected content and communicate with each other through pointing gestures [42, 50, 52]. However, in this scenario, the projection light is occluded by multiple users' bodies, and the resulting shadows hinder task execution. Furthermore, the low spatial resolution and contrast in the projected results may decrease the user's visibility and impede task performance. Therefore, we compared task performance, in terms of completion time and number of mistakes, across multiple projection conditions for a specific task.

The projection conditions we compared included standard projection, LA projection, and proposed projection. In the LA projection, we employed our proposed model for blur compensation. We used the OursBalance condition (cf. subsection 5.4) in the proposed projection. We formulated the following hypotheses for this study:

H1 A user completes tasks in the proposed projection faster than the standard projection and the LA projection.

H2 A user has fewer mistakes in the proposed projection than the standard projection and the LA projection.

6.1 Experimental setup and procedure

To conduct the study, we modified the experimental setup used in section 5. Figure 6 (b) and (c) show the schematic diagram and actual photos of the modified setup. We used a pen tablet (Wacom, Bamboo CTH-670/K) as the projection target. The participants used the accompanying pen to interact with the projected images. To make it easier for the participants to work while seated, we reflected the projection light with a mirror and projected the images vertically downward onto the pen tablet, which was placed on a tabletop.

Task: During the experiment, the participants were given a tracing task based on the instructions displayed in the images (see Figure 6 (a) for an example image). The participants were asked to trace large characters within a 6×5 block, following the order of the small letters displayed at the top of the image. They were only allowed to move vertically or horizontally between blocks. If they correctly traced a block, it turned uniform black. However, if they touched the wrong block, the image reset to its initial state and they needed to trace again from the starting point. In total, the participants traced 18 characters, including the starting point.

We recorded the completion time and the number of mistakes for each participant. In addition, considering scenarios where multiple users would be using the PM system, such as surgical assistance PM systems, we placed an external occluder separate from the participant. The projected results included shadows caused by the occluder as well as shadows from the participants' hands and the pen they were holding. We used a wooden hand (finger width 10 mm) as the occluder, positioned 150 mm away from the Fresnel lens. Since the occluder

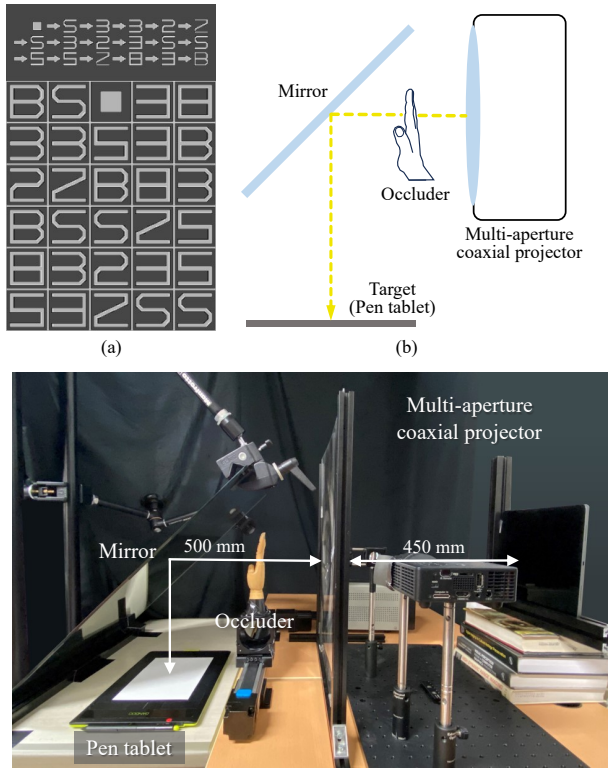

Fig. 6: Setup for user study. (a) An example of projected image used in the user study. (b) Conceptual diagram of the setup. (c) Implemented system.

was positioned to imitate a moving user rather than a fixed object, we moved it horizontally at a speed of 10 mm per second using a linear stage.

The experiment involved 27 participants aged 21 to 54, consisting of 17 males and 10 females. All participants had normal or corrected vision and were naïve to the purpose of the experiment, having given informed consent. Before the experiment, the participants were briefed on the task and had sufficient practice for each condition. They were instructed to record both the task completion time and the number of mistakes, with no specified priority between the two. The participants practiced the task thoroughly for each projection condition and developed an optimal strategy for balancing completion time and number of mistakes. The experiment consisted of four trials for each condition, and the order of images and projection conditions was randomly changed for each participant.

After completing the entire experiment, the participants were asked to complete a questionnaire related to each task. The questions were as follows:

Q.1 Do you agree that the shadow of the external occluder inhibited task execution?

Q.2 Do you agree that the self shadows cast by the your own hands or pens inhibited task execution?

Q.3 Do you agree that the clarity of the image was insufficient for task execution?

Q.4 Under which condition was it easiest to perform the task?

Q.5 Which condition inhibited task execution more: "shadows cast by occluders" or "unclarity of the image"?

Participants answered questions Q.1 to Q.3 using a 7-point Likert scale for all three conditions, where 3 represented "strongly agree" and -3 represented "strongly disagree". The study was approved by the Research Ethics Review Committee of the institute to which the

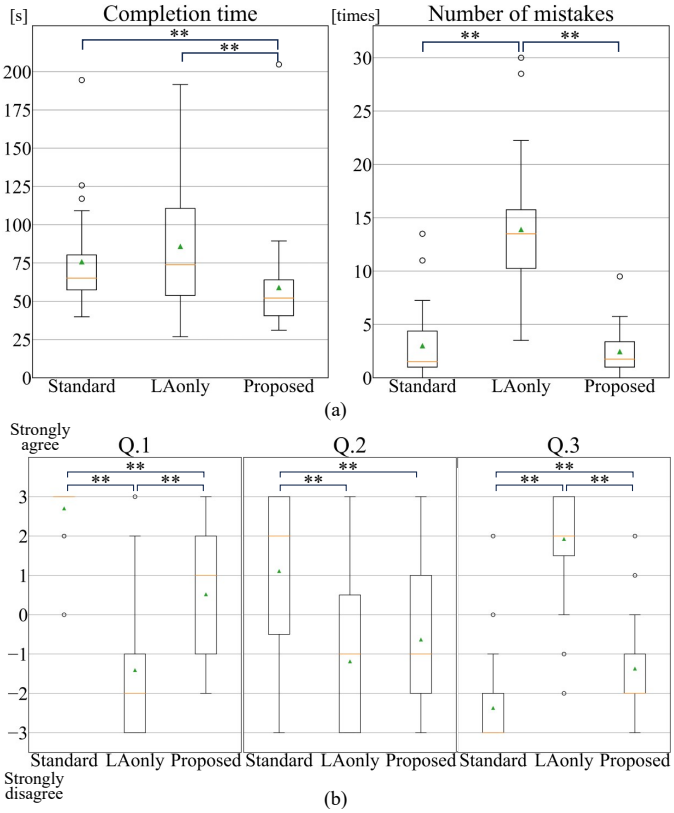

Fig. 7: Results of the user study under different projection conditions. (a) Comparison of task completion time and number of mistakes. (b) Comparison of questionnaire results. ($** : p < 0.01$)

corresponding author belongs (approval number; R5-3).

6.2 Results

The results of task completion time and number of mistakes under each projection condition are shown in Figure 7(a). In the subsequent statistical tests, we used nonparametric tests to address the impact of outliers. Friedman tests were conducted on completion time as a factor of projection conditions, revealing a significant difference ($\chi^2(2) = 27.0, p < 0.01$). Wilcoxon signed-rank tests with Bonferroni correction revealed significant differences between the standard projection and the proposed method ($p < 0.01$, Effect size: $r = 0.82$, Power: $1-\beta = 0.91$), and between the LA projection and the proposed method ($p < 0.01$, $r = 0.62$, $1-\beta = 0.65$). The proposed method suggested significantly shorter task completion times compared to other conditions.

Regarding the number of mistakes, Friedman tests showed a significant difference ($\chi^2(2) = 40.9, p < 0.01$). Wilcoxon signed-rank tests with Bonferroni correction revealed significant differences between the standard projection and the LA projection ($p < 0.01$, $r = 0.87$, $1-\beta = 0.94$), as well as between the LA projection and the proposed method ($p < 0.01$, $r = 0.87$, $1-\beta = 0.94$). The proposed method indicated a significantly lower number of mistakes compared to the LA projection.

Figure 7(b) shows the results for questions Q.1 to Q.3 under each projection condition. Friedman tests showed significant differences for all questions (Q.1: $\chi^2(2) = 42.9$, Q.2: $\chi^2(2) = 21.0$, Q.3: $\chi^2(2) = 46.0$, $p < 0.01$). Wilcoxon signed-rank tests with Bonferroni correction revealed that, for Q.1 and Q.2, both the LA projection and the proposed method significantly reduced task interference due to shadows compared to the standard projection. Additionally, for Q.3, both the standard projection and the proposed method significantly reduced task interference due to image blurriness compared to the LA projection.

For Q.4, out of 27 participants, 25 found the proposed method to be the most user-friendly for task execution, while 2 chose the standard projection. Regarding Q.5, 22 out of 27 participants indicated that "unclarity" more significantly inhibited the task, while 5 mentioned that "shadows" had a greater impact. This result indicates that visibility of the small texts showing the tracing order displayed at the top of the image was prioritized.

Both objective measures (task completion time and number of mistakes), and subjective evaluation suggested that cast shadows and unclear images inhibited task execution. The proposed method achieves a balance between these factors, allowing tasks to be performed more quickly and with fewer mistakes. Thus, the result provides substantial evidence suggesting that the proposed method has the potential to enhance user task performance in interactive PM systems.

7 Discussion

We have demonstrated the effectiveness of our proposed shadow suppressible PM system through simulations, projection experiments, and a user study. First, we accurately modeled the degradation process of projection with an LA Fresnel lens and verified its validity in subsection 5.3. Next, we generated the pair of projection images, and showed that blur compensation was achieved while maintaining the shadow suppression performance in subsection 5.4. Finally, user studies suggest that the proposed method has the potential to improve performance on certain tasks compared to standard projection or LA projection alone in section 6. Note that we cannot say that the results represent a trend for humanity as a whole. Since our institute is located in Japan, where racial diversity is relatively low, conducting our experiments with non-Japanese participants is difficult. Although the proposed method has been validated, there are technical issues that remain in the current prototypes and methods. In the remainder of this section, we will describe the specific challenges and their potential solutions, and provide guidelines for future development.

Compared to commonly used office projectors, the image size that our PM system can project is small (Max. height: 233 mm, width: 304 mm). Most projectors enlarge the image size by employing a short focal length system, which combines multiple lenses. Similarly, in our system, it can be considered to incorporate additional optics, such as a relay lens system, into the LA projector alongside the LA Fresnel lens. However, using multiple Fresnel lenses in LA projectors is not reasonable due to the problems of veiling glare and stray light on image quality. The simplest approach is to shorten the distance between the light source and the lens, bringing it close to the focal length of the lens. However, this results in a longer focusing distance, and thus, the projection light is condensed from a narrow viewing angle onto a point on the projection surface. This leads to a reduction in shadow suppression performance. Future challenges for our research are to investigate the angular range within which users tolerate shadows, and to find the appropriate image size and solid angle for individual applications.

An optical system employing LA lenses suffers from a shallow DOF. While the proposed system utilizes a deblurring method to extend the DOF, the realistic range of the projected object in the depth direction is still limited. To overcome the limitation, previous studies have proposed optical solutions to extend the DOF, such as using an electrical focus tunable lens [19, 63] and a diffractive optical element [35]. However, these optical elements are generally too small to be used as objective lenses in our LA projector. Another potential solution is to adjust the lens position based on the depth of the projection surface, or utilizing a volumetric display as a light source module of the LA projector [31, 32, 44]. These approaches can be employed in our system to extend its DOF. Exploring the DOF extension would be one of our future directions.

We proposed an optimization framework in generating projection images to minimize the artifacts in the projected results. However, this optimization requires a long calculation time. Other studies on projector deblurring share this limitation, and it can be a significant constraint when applying it to dynamic 3D PM applications. In our implementation, our method takes 0.33 seconds to obtain one pair of projection images as the output of the optimization solver, and 8.2

seconds to generate one pair of representative images at a given depth, in a monochrome image of 128 × 128 pixels. Currently, the prototype is unable to project a compensation image in real-time. Recent studies have achieved real-time generation of optimized projection images by applying deep neural networks [28, 36, 64]. It is an intriguing direction for future research to explore the potential of real-time compensation using deep neural networks.

8 Conclusion

In this paper, we presented an optical, and thus, delay-free shadow suppression PM system utilizing the LA Fresnel lens. To address the image quality degradation in the LA projection, we implemented optical and digital image processing methods. Firstly, we introduced a residual projector along the same optical axis as the LA projector to compensate for high-frequency components attenuated in the LA projection. Secondly, we generated optimized projection images for the LA projector and residual projector, which compensate for the blur in the projected results while maximizing the shadow suppression performance. In this compensation process, we utilized the novel degradation model that can more accurately represent the projected result using an LA Fresnel lens. Through simulations and projection experiments, we validated these proposals. Additionally, user studies showed that our system could decrease the task completion time and error rates for a specific interactive PM task compared to other types of PM systems.

We believe that our method has the potential to enhance the user experience in various interactive PM applications. We plan to further improve the system by addressing future directions discussed in section 7 to achieve a more practical and widely applicable shadow suppression PM system.

Acknowledgments

This work was supported by JSPS KAKENHI grant number JP20H05958, JST PRESTO Grant Number JPMJPR19J2, and the Future Social Value Co-Creation Project, Osaka University.

References

[1] S. Audet and J. R. Cooperstock. Shadow removal in front projection environments using object tracking. In *2007 IEEE Conference on Computer Vision and Pattern Recognition*, pp. 1–8, 2007. 2

[2] D. Bandyopadhyay, R. Raskar, and H. Fuchs. Dynamic shader lamps : painting on movable objects. In *Proceedings IEEE and ACM International Symposium on Augmented Reality*, pp. 207–216, 2001. 1

[3] K. Bang, Y. Jo, M. Chae, and B. Lee. Lenslet vr: thin, flat and wide-fov virtual reality display using fresnel lens and lenslet array. *IEEE Transactions on Visualization and Computer Graphics*, 27(5):2545–2554, 2021. 2

[4] A. H. Bermano, M. Billeter, D. Iwai, and A. Grundhöfer. Makeup lamps: Live augmentation of human faces via projection. *Computer Graphics Forum*, 36(2):311–323, 2017. 1

[5] O. Bimber, F. Coriand, A. Kleppe, E. Bruns, S. Zollmann, and T. Langlotz. Superimposing pictorial artwork with projected imagery. *IEEE MultiMedia*, 12(1):16–26, 2005. 1

[6] O. Bimber and R. Raskar. *Spatial Augmented Reality: Merging Real and Virtual Worlds*. A. K. Peters, Ltd., 2005. 1

[7] M. S. Brown, P. Song, and T.-J. Cham. Image pre-conditioning for out-of-focus projector blur. In *2006 IEEE Computer Society Conference on Computer Vision and Pattern Recognition (CVPR'06)*, vol. 2, pp. 1956–1963. IEEE, 2006. 2, 3, 5

[8] G. Cascini, J. O'Hare, E. Dekoninck, N. Becattini, J.-F. Boujut, F. Ben Guefrache, I. Carli, G. Caruso, L. Giunta, and F. Morosi. Exploring the use of ar technology for co-creative product and packaging design. *Computers in Industry*, 123:103308, 2020. 1

[9] J. Deng, W. Dong, R. Socher, L.-J. Li, K. Li, and L. Fei-Fei. Imagenet: A large-scale hierarchical image database. In *2009 IEEE conference on computer vision and pattern recognition*, pp. 248–255. Ieee, 2009. 6

[10] K. Ding, K. Ma, S. Wang, and E. P. Simoncelli. Image quality assessment: Unifying structure and texture similarity. *CoRR*, abs/2004.07728, 2020. 7

[11] P. Favaro and S. Soatto. A geometric approach to shape from defocus. *IEEE Transactions on Pattern Analysis and Machine Intelligence*, 27(3):406–417, 2005. 3

[12] M. Flagg and J. M. Rehg. Projector-guided painting. In *Proceedings of the 19th Annual ACM Symposium on User Interface Software and Technology*, 10 pages, p. 235–244, 2006. 1

[13] K. Fujii, M. D. Grossberg, and S. K. Nayar. A projector-camera system with real-time photometric adaptation for dynamic environments. In *2005 IEEE Computer Society Conference on Computer Vision and Pattern Recognition (CVPR'05)*, vol. 1, pp. 814–821. IEEE, 2005. 3

[14] Y. Geng, J. Gollier, B. Wheelwright, F. Peng, Y. Sulai, B. Lewis, N. Chan, W. S. T. Lam, A. Fix, D. Lanman, et al. Viewing optics for immersive near-eye displays: pupil swim/size and weight/stray light. In *Digital Optics for Immersive Displays*, vol. 10676, pp. 19–35. SPIE, 2018. 2, 4

[15] H. Haitao, D. Ruijun, H. Na, B. Jiarong, W. Yulong, L. Ke, W. Chenru, M. Zhanshan, C. Lili, and Z. hao. 63-2: Research on stray light affecting the imaging of fresnel lens in virtual reality equipment. In *SID Symposium Digest of Technical Papers*, vol. 53, pp. 827–829. Wiley Online Library, 2022. 2

[16] K. Hiratani, D. Iwai, Y. Kageyama, P. Punpongsanon, T. Hiraki, and K. Sato. Shadowless projection mapping using retrotransmissive optics. *IEEE Transactions on Visualization and Computer Graphics*, 29(5):2280–2290, 2023. 2

[17] K. Hiratani, D. Iwai, P. Punpongsanon, and K. Sato. Shadowless projector: Suppressing shadows in projection mapping with micro mirror array plate. In *2019 IEEE Conference on Virtual Reality and 3D User Interfaces (VR)*, pp. 1309–1310, 2019. doi: 10.1109/VR.2019.8798245 2

[18] D. Iwai, R. Matsukage, S. Aoyama, T. Kikukawa, and K. Sato. Geometrically consistent projection-based tabletop sharing for remote collaboration. *IEEE Access*, 6:6293–6302, 2018. 1

[19] D. Iwai, S. Mihara, and K. Sato. Extended depth-of-field projector by fast focal sweep projection. *IEEE transactions on visualization and computer graphics*, 21(4):462–470, 2015. 9

[20] D. Iwai, M. Nagase, and K. Sato. Shadow removal of projected imagery by occluder shape measurement in a multiple overlapping projection system. *Virtual Reality*, 18(4):245–254, Nov 2014. 1, 2

[21] D. Iwai and K. Sato. Limpid desk: See-through access to disorderly desktop in projection-based mixed reality. In *Proceedings of the ACM Symposium on Virtual Reality Software and Technology*, VRST '06, 4 pages, p. 112–115. Association for Computing Machinery, New York, NY, USA, 2006. doi: 10.1145/1180495.1180519 1

[22] D. Iwai and K. Sato. Document search support by making physical documents transparent in projection-based mixed reality. *Virtual Reality*, 15(2):147–160, Jun 2011. 1

[23] C. Jaynes, S. Webb, and R. Steele. Camera-based detection and removal of shadows from interactive multiprojector displays. *IEEE Transactions on Visualization and Computer Graphics*, 10(3):290–301, 2004. 1, 2

[24] C. Jaynes, S. Webb, R. Steele, M. Brown, and W. Seales. Dynamic shadow removal from front projection displays. In *Proceedings Visualization, 2001. VIS '01.*, pp. 175–555, 2001. 1, 2

[25] C. Jiang, Y. Omuro, J. She, J. Nan, and M. Liu. Improving the quality of fresnel vr lenses by creating extra room for trapped air and evaluating slope angle. *Optik*, 288:171200, 2023. 2

[26] Y. Kageyama, M. Isogawa, D. Iwai, and K. Sato. Prodebnet: projector deblurring using a convolutional neural network. *Opt. Express*, 28(14):20391–20403, Jul 2020. doi: 10.1364/OE.396159 2, 3

[27] Y. Kageyama, D. Iwai, and K. Sato. Online projector deblurring using a convolutional neural network. *IEEE Transactions on Visualization and Computer Graphics*, 28(5):2223–2233, 2022. doi: 10.1109/TVCG.2022.3150465 2, 3

[28] Y. Kageyama, D. Iwai, and K. Sato. Efficient distortion-free neural projector deblurring in dynamic projection mapping. *IEEE Transactions on Visualization and Computer Graphics*, 2024. 10

[29] J. Kim, H. Seo, S. Cha, and J. Noh. Real-time human shadow removal in a front projection system. *Computer Graphics Forum*, 38(1):443–454, 2019. 1, 2

[30] Y. Kitajima, D. Iwai, and K. Sato. Simultaneous projection and positioning of laser projector pixels. *IEEE Transactions on Visualization and Computer Graphics*, 23(11):2419–2429, 2017. 1

[31] M. Kiyokawa and N. Hashimoto. Dynamic projection mapping with 3d images using volumetric display. In *2021 IEEE Conference on Virtual Reality and 3D User Interfaces Abstracts and Workshops (VRW)*, pp. 597–598, 2021. doi: 10.1109/VRW52623.2021.00181 9

[32] M. Kiyokawa, S. Okuda, and N. Hashimoto. Stealth projection: Visually removing projectors from dynamic projection mapping. In *SIGGRAPH Asia 2019 Posters*, SA '19, article no. 41, 2 pages. Association for Com-

puting Machinery, New York, NY, USA, 2019. doi: 10.1145/3355056.3364551 2, 9

[33] D. J. Lamb and L. W. Hillman. Computer modeling and analysis of veiling glare and stray light in fresnel lens optical system. In *Current Developments in Optical Design and Optical Engineering VIII*, vol. 3779, pp. 344–352. SPIE, 1999. 2

[34] M. Levoy, B. Chen, V. Vaish, M. Horowitz, I. McDowall, and M. Bolas. Synthetic aperture confocal imaging. *ACM Trans. Graph.*, 23(3):825–834, 10 pages, Aug. 2004. 2

[35] Y. Li, Q. Fu, and W. Heidrich. Extended depth-of-field projector using learned diffractive optics. In *2023 IEEE Conference Virtual Reality and 3D User Interfaces (VR)*, pp. 449–459. IEEE, 2023. 9

[36] Y. Li, W. Yin, J. Li, and X. Xie. Physics-based efficient full projector compensation using only natural images. *IEEE Transactions on Visualization and Computer Graphics*, 2023. 10

[37] M. R. Marner, R. T. Smith, J. A. Walsh, and B. H. Thomas. Spatial user interfaces for large-scale projector-based augmented reality. *IEEE Computer Graphics and Applications*, 34(6):74–82, 2014. 1

[38] D. W. Marquardt. An algorithm for least-squares estimation of nonlinear parameters. *Journal of the society for Industrial and Applied Mathematics*, 11(2):431–441, 1963. 6

[39] K. Matsushita, D. Iwai, and K. Sato. Interactive bookshelf surface for in situ book searching and storing support. In *Proceedings of the 2nd Augmented Human International Conference*, article no. 2, 8 pages, 2011. 1

[40] C. Menk, E. Jundt, and R. Koch. Visualisation techniques for using spatial augmented reality in the design process of a car. *Computer Graphics Forum*, 30(8):2354–2366, 2011. 1

[41] M. Nagase, D. Iwai, and K. Sato. Dynamic defocus and occlusion compensation of projected imagery by model-based optimal projector selection in multi-projection environment. *Virtual Reality*, 15(2):119–132, Jun 2011. 1, 2

[42] H. Nishino, E. Hatano, S. Seo, T. Nitta, T. Saito, M. Nakamura, K. Hattori, M. Takatani, H. Fuji, K. Taura, and S. Uemoto. Real-time navigation for liver surgery using projection mapping with indocyanine green fluorescence: Development of the novel medical imaging projection system. *Annals of Surgery*, 267(6):1134–1140, 2018. 1, 8

[43] T. Nomoto, W. Li, H.-L. Peng, and Y. Watanabe. Dynamic projection mapping with networked multi-projectors based on pixel-parallel intensity control. In *SIGGRAPH Asia 2020 Emerging Technologies*, article no. 11, 2 pages, 2020. 1, 2

[44] S. Okuda and N. Hashimoto. Projection mapping using a rotating volumetric 3D display. In M. Nakajima, J.-G. Kim, W.-N. Lie, and Q. Kemao, eds., *International Workshop on Advanced Imaging Technology (IWAIT) 2021*, vol. 11766, pp. 334 – 339. International Society for Optics and Photonics, SPIE, 2021. doi: 10.1117/12.2591029 9

[45] Y. Oyamada and H. Saito. Focal pre-correction of projected image for deblurring screen image. In *2007 IEEE Conference on Computer Vision and Pattern Recognition*, pp. 1–8. IEEE, 2007. 2, 3

[46] T. Pejsa, J. Kantor, H. Benko, E. Ofek, and A. Wilson. Room2room: Enabling life-size telepresence in a projected augmented reality environment. In *Proceedings of the 19th ACM Conference on Computer-Supported Cooperative Work and Social Computing*, CSCW '16, 10 pages, p. 1716–1725, 2016. 1

[47] R. Raskar, P. Beardsley, J. van Baar, Y. Wang, P. Dietz, J. Lee, D. Leigh, and T. Willwacher. Rfig lamps: Interacting with a self-describing world via photosensing wireless tags and projectors. *ACM Trans. Graph.*, 23(3):406–415, 10 pages, Aug. 2004. 1

[48] R. Raskar, G. Welch, M. Cutts, A. Lake, L. Stesin, and H. Fuchs. The office of the future: A unified approach to image-based modeling and spatially immersive displays. In *Proceedings of the 25th Annual Conference on Computer Graphics and Interactive Techniques*, SIGGRAPH '98, 10 pages, p. 179–188, 1998. 1

[49] A. Rivers, A. Adams, and F. Durand. Sculpting by numbers. *ACM Trans. Graph.*, 31(6), article no. 157, 7 pages, Nov. 2012. 1

[50] L. Rodriguez, F. Quint, D. Gorecky, D. Romero, and H. R. Siller. Developing a mixed reality assistance system based on projection mapping technology for manual operations at assembly workstations. *Procedia computer science*, 75:327–333, 2015. 8

[51] T. Sakai. Light-shielding film on edges and draft facets of fresnel lens fabricated by picosecond laser processing. *Optical Review*, 26(5):447–451, 2019. 2

[52] O. Sand, S. Büttner, V. Paelke, and C. Röcker. smart. assembly–projection-based augmented reality for supporting assembly workers. In *Virtual, Augmented and Mixed Reality: 8th International Conference, VAMR 2016, Held as Part of HCI International 2016, Toronto, Canada, July 17-22, 2016. Proceedings 8*, pp. 643–652. Springer, 2016. 8

[53] S. Schmidt, G. Bruder, and F. Steinicke. Effects of virtual agent and object representation on experiencing exhibited artifacts. *Computers & Graphics*, 83:1 – 10, 2019. 1

[54] P. Sen, B. Chen, G. Garg, S. R. Marschner, M. Horowitz, M. Levoy, and H. P. Lensch. Dual photography. In *ACM SIGGRAPH 2005 Papers*, pp. 745–755. 2005. 3

[55] C. Siegl, V. Lange, M. Stamminger, F. Bauer, and J. Thies. Faceforge: Markerless non-rigid face multi-projection mapping. *IEEE Transactions on Visualization and Computer Graphics*, 23(11):2440–2446, 2017. 1

[56] Y. Sugaya, I. Miyagawa, and H. Koike. Contrasting shadow for occluder light suppression from one-shot image. In *2010 IEEE Computer Society Conference on Computer Vision and Pattern Recognition - Workshops*, pp. 96–103, 2010. 2

[57] R. Sukthankar, T.-J. Cham, and G. Sukthankar. Dynamic shadow elimination for multi-projector displays. In *Proceedings of the 2001 IEEE Computer Society Conference on Computer Vision and Pattern Recognition. CVPR 2001*, vol. 2, pp. II–II, 2001. 1, 2

[58] J. Summet, G. D. Abowd, G. M. Corso, and J. M. Rehg. Virtual rear projection: Do shadows matter? In *CHI '05 Extended Abstracts on Human Factors in Computing Systems*, 4 pages, p. 1997–2000, 2005. 1

[59] T. Takezawa, D. Iwai, K. Sato, T. Hara, Y. Takeda, and K. Murase. Material surface reproduction and perceptual deformation with projection mapping for car interior design. In *2019 IEEE Conference on Virtual Reality and 3D User Interfaces (VR)*, pp. 251–258, 2019. 1

[60] J. Tsukamoto, D. Iwai, and K. Kashima. Radiometric compensation for cooperative distributed multi-projection system through 2-dof distributed control. *IEEE Transactions on Visualization and Computer Graphics*, 21(11):1221–1229, 2015. 1, 2

[61] J. Tsukamoto, D. Iwai, and K. Kashima. Distributed optimization framework for shadow removal in multi-projection systems. *Computer Graphics Forum*, 36(8):369–379, 2017. 1, 2

[62] J. Underkoffler and H. Ishii. Urp: A luminous-tangible workbench for urban planning and design. In *Proceedings of the SIGCHI Conference on Human Factors in Computing Systems*, 8 pages, p. 386–393, 1999. 1

[63] L. Wang, S. Tabata, H. Xu, Y. Hu, Y. Watanabe, and M. Ishikawa. Dynamic depth-of-field projection mapping method based on a variable focus lens and visual feedback. *Optics Express*, 31(3):3945–3953, 2023. 9

[64] Y. Wang, H. Ling, and B. Huang. Vicomp: Video compensation for projector-camera systems. *IEEE Transactions on Visualization and Computer Graphics*, 2024. 10

[65] Z. Wang, A. C. Bovik, H. R. Sheikh, and E. P. Simoncelli. Image quality assessment: from error visibility to structural similarity. *IEEE transactions on image processing*, 13(4):600–612, 2004. 7

[66] G. Wetzstein and O. Bimber. Radiometric compensation through inverse light transport. Technical report, Junior-Professur Augmented Reality, 2007. 3

[67] K. Yamamoto, D. Iwai, I. Tani, and K. Sato. A monocular projector-camera system using modular architecture. *IEEE Transactions on Visualization and Computer Graphics*, 2022. 3

[68] T. Yoshida, C. Horii, and K. Sato. A virtual color reconstruction system for real heritage with light projection. In *Proceedings of VSMM*, vol. 3, pp. 1–7. Citeseer, 2003. 7

[69] L. Zhang and S. Nayar. Projection defocus analysis for scene capture and image display. In *ACM SIGGRAPH 2006 Papers*, pp. 907–915. 2006. 2, 3, 4, 5, 6, 7